DOI: 10.13009/EUCASS2017-192

Robust Control Augmentation System for Flight Envelope Protection Using Backstepping Control Scheme

Yongjun Seo⋆ *and Youdan Kim*⋆†
⋆*Department of Mechanical and Aerospace Engineering*
Seoul National University, Seoul, Republic of Korea, 151-742
tomcat14@snu.ac.kr · ydkim@snu.ac.kr
†Corresponding Author

Abstract

Most critical aircraft Loss-of-Control (LoC) is caused by the excursion of aerodynamic angles that exceed the flight envelope. Therefore, aerodynamic angles such as angle of attack (AOA) and sideslip angle, and normal load factor must be kept within a flight envelope during the flight to prevent LoC. In this study, a model-based robust control augmentation system (CAS) with Flight Envelope Protection (FEP) scheme based on pilot command limiting method is proposed. A backstepping tracking controller with control allocation is designed, which makes the aircraft robustly track the roll rate, AOA, and sideslip angle commands. Pilot stick and pedal inputs are assigned as roll rate and angle commands using appropriate nonlinear mapping. Proper selection of control gains ensures ultimate boundedness of the tracking error considering the saturation of actuators. Normal load factor envelope is also protected by limiting the AOA command where the normal load factor mainly accounts for the structural integrity of the aircraft. Numerical simulation results demonstrate the performance of the proposed CAS.

1. Introduction

Loss-of-Control(LoC) is the main cause of the fatal aircraft accidents, and thus, there have been enormous efforts to classify the type of LoC and develop control laws that reduce its occurrence. To investigate the quantitative factors that induce the LoC, various works[1,2] have been performed. As a result, it was shown that LoC is typically attributed to the excursion of important states such as angle of attack and sideslip angle exceeding safe flight envelope which is dependent on the aircraft model. The flight envelope approach is proven to be reliable according to the works of Wilborn et al.,[1] who developed a quantitative method to define LoC based on commercial passenger accident data and flight test data. The study was continued by Chongvisal et al.,[2] where the flight envelope is adjusted in real time based on the flight conditions.

Once the safe flight envelope is defined for a specified aircraft, the flight envelope can be protected by integrating the LoC detection logic and a flight control law. Numerous flight control logics that have reliability and robustness against aerodynamic uncertainty have been proposed. Among the control logics, backstepping control scheme is a quite effective method in that it provides a systematic way to deal with the unmatched uncertainty which is common in the aircraft dynamics.[3,4] However, it is not easy to design a flight control system that includes the FEP functionality due to aerodynamic complexity. As an expedient, the integration problem is often handled by solving its subproblems: to separate each flight condition and apply gain scheduling, to decouple the system into relatively small systems, for instance, lateral and longitudinal dynamics.[5] Another approach preferred in the literature utilizes a neural networks, where the neural network can be trained to calculate the control deflections to avoid the flight envelope exceedance.[6]

In this study, a robust flight controller with FEP logic is proposed. The flight envelope approach is one of the most effective and intuitive way to detect the onset and estimate its severity. The primary goal of FEP is to prevent the onset of LoC caused by aircraft upset. To meet the requirement, pilot's command signals, i.e. stick and rudder pedal, are carefully mapped to the roll rate and the aerodynamic angles. The mapping gives commands that are included in safe flight envelope. Then, a robust controller is designed based on backstepping control scheme. The controller can always track the commanded input under some bounded aerodynamic uncertainty. To simplify the controller design and properly cover the actuator redundancy and physical limitations such as angle saturation and rate limit, an effective control allocator is designed.

DOI: 10.13009/EUCASS2017-192

The paper is organized as follows; first, the aircraft model is introduced in Sec. 2. In Sec. 3, the design and the practical application of control allocation scheme are explained. The backstepping-based controller is designed in Sec. 4, and Sec. 5 provides the simulation result. Finally, the conclusions are given in Sec. 6.

2. Aircraft Model

2.1 Aerodynamics

F/A-18 High Angle of attack Research Vehicle (HARV) is selected as an aircraft model, which consists of the lookup table containing aerodynamic derivative coefficients as functions of angle of attack. The valid angle of attack ranges from -14° to 90°. The aerodynamic coefficients are represented as follows.

$$\begin{aligned} C_L &= C_{L_0} + C_{L_Q} Q\,(\bar{c}/2V_T) + C_{L_{\delta_{el}}}\delta_{el} + C_{L_{\delta_{er}}}\delta_{er} \\ C_Y &= C_{Y_\beta}\beta + (C_{Y_P}P + C_{Y_R}R)\,(b/2V_T) + C_{Y_{\delta_{el}}}\delta_{el} + C_{Y_{\delta_{er}}}\delta_{er} + C_{Y_{\delta_a}}\delta_a + C_{Y_{\delta_r}}\delta_r \\ C_D &= C_{D_0} + C_{D_Q} Q\,(\bar{c}/2V_T) + C_{D_{\delta_{el}}}\delta_{el} + C_{D_{\delta_{er}}}\delta_{er} \end{aligned} \tag{1}$$

$$\begin{aligned} C_l &= C_{l_\beta}\beta + (C_{l_P}P + C_{l_R}R)\,(b/2V_T) + C_{l_{\delta_{el}}}\delta_{el} + C_{l_{\delta_{er}}}\delta_{er} + C_{l_{\delta_a}}\delta_a + C_{l_{\delta_r}}\delta_r \\ C_m &= C_{m_0} + C_{m_Q} Q\,(\bar{c}/2V_T) + C_{m_{\delta_{el}}}\delta_{el} + C_{m_{\delta_{er}}}\delta_{er} \\ C_n &= C_{n_\beta}\beta + (C_{n_P}P + C_{n_R}R)\,(b/2V_T) + C_{n_{\delta_{el}}}\delta_{el} + C_{n_{\delta_{er}}}\delta_{er} + C_{n_{\delta_a}}\delta_a + C_{n_{\delta_r}}\delta_r \end{aligned} \tag{2}$$

The corresponding force coefficients can be obtained by coordinate transformation from wind axes to body axes as

$$\mathbf{C}_F = \mathbf{C}_{b/w}\,[-C_D\ C_Y\ -C_L]^\top \tag{3}$$

where

$$\mathbf{C}_{b/w} = \begin{bmatrix} \cos\alpha\cos\beta & \sin\beta & \sin\alpha\cos\beta \\ -\cos\alpha\sin\beta & \cos\beta & -\sin\alpha\sin\beta \\ -\sin\alpha & 0 & \cos\alpha \end{bmatrix}^\top \tag{4}$$

Then, the aerodynamic force and moment exerted on the aircraft can be expressed as

$$\mathbf{F}_A = [X\ Y\ Z]^\top = qS\,\mathbf{C}_F \tag{5}$$

$$\mathbf{E}_A = [L\ M\ N]^\top = qS\mathbf{B}\mathbf{C}_M \tag{6}$$

where $q = \frac{1}{2}\rho V^2$, $\mathbf{B} = \mathrm{diag}\,(b, \bar{c}, b)$, and $\mathbf{C}_M = [C_l\ C_m\ C_n]^\top$. Particularly, the aerodynamic moment is affine in the control surface input as

$$\mathbf{C}_M = \mathbf{C}_0 + \mathbf{C}_\delta\boldsymbol{\delta} \tag{7}$$

where

$$\mathbf{C}_0 = \begin{bmatrix} C_{l_\beta}\beta + (C_{l_P}P + C_{l_R}R)\,(b/2V_T) \\ C_{m_0} + C_{m_Q} Q\,(\bar{c}/2V_T) \\ C_{n_\beta}\beta + (C_{n_P}P + C_{n_R}R)\,(b/2V_T) \end{bmatrix},\ \mathbf{C}_\delta = \begin{bmatrix} C_{l_{\delta_{el}}} & C_{l_{\delta_{er}}} & C_{l_{\delta_a}} & C_{l_{\delta_r}} \\ C_{m_{\delta_{el}}} & C_{m_{\delta_{er}}} & 0 & 0 \\ C_{n_{\delta_{el}}} & C_{n_{\delta_{er}}} & C_{n_{\delta_a}} & C_{n_{\delta_r}} \end{bmatrix} \tag{8}$$

and $\boldsymbol{\delta} = [\delta_{el}\ \delta_{er}\ \delta_a\ \delta_r]^\top$. In this study, by introducing $\mathbf{E}_0 = \mathbf{B}\mathbf{C}_0$ and $\mathbf{E} = \mathbf{B}\mathbf{C}_\delta$, the aerodynamic moment coefficients are combined to simplify the model. as

$$\mathbf{E}_A = \mathbf{E}_A\,(\boldsymbol{\delta}) = \mathbf{E}_0 + \mathbf{E}\boldsymbol{\delta} \tag{9}$$

The matrix $\mathbf{E}$ is called an effectiveness matrix.

2.2 Equations of Motion

The state variables used for the aircraft model are $\boldsymbol{\omega} = [P\ Q\ R]^\top$, $\mathbf{x}_2 = [\mu\ \beta\ \alpha]^\top$, and $\mathbf{x}_3 = [\gamma\ V]^\top$ and the inputs are δ_t and $\boldsymbol{\delta}$. Using these variables, the nominal equations of motion of the aircraft can be written as follows.

$$\dot{\boldsymbol{\omega}} = \mathbf{J}^{-1}\,(qS\,\mathbf{E}_A - \boldsymbol{\Omega}\mathbf{J}\boldsymbol{\omega}) \tag{10}$$

$$\dot{\mu} = f_\mu\,(\mathbf{x}, \boldsymbol{\delta}) + \mathbf{g}_\mu{}^\top\boldsymbol{\omega} \tag{11a}$$

$$\dot{\beta} = f_\beta\,(\mathbf{x}, \boldsymbol{\delta}) + \mathbf{g}_\beta{}^\top\boldsymbol{\omega} \tag{11b}$$

$$\dot{\alpha} = f_\alpha\,(\mathbf{x}, \boldsymbol{\delta}) + \mathbf{g}_\alpha{}^\top\boldsymbol{\omega} \tag{11c}$$

DOI: 10.13009/EUCASS2017-192

$$\dot{\mathbf{x}}_3 = \mathbf{f}_3(\mathbf{x}, \boldsymbol{\delta}) \tag{12}$$

where $\mathbf{f}_3 = \left[f_\gamma \; f_V\right]^\top$ and

$$f_\mu = \frac{1}{mV}\left\{Y\cos\mu\tan\gamma + L(\tan\beta + \sin\mu\tan\gamma) + T_\mu\right\} + \frac{g_\mu}{V} \tag{13a}$$

$$f_\beta = \frac{1}{mV}\left(Y + T_\beta\right) + \frac{g_\beta}{V} \tag{13b}$$

$$f_\alpha = \frac{1}{mV\cos\beta}(-L + T_\alpha) + \frac{g_\alpha}{V}\sin\alpha\tan\beta \tag{13c}$$

$$\mathbf{g}_\mu = \left[\frac{\cos\alpha}{\cos\beta} \; 0 \; \frac{\sin\alpha}{\cos\beta}\right]^\top \tag{14a}$$

$$\mathbf{g}_\beta = [\sin\alpha \; 0 \; -\cos\alpha]^\top \tag{14b}$$

$$\mathbf{g}_\alpha = [-\cos\alpha\tan\beta \; 1 \; -\sin\alpha\tan\beta]^\top \tag{14c}$$

$$f_\gamma = \frac{1}{mV}\{L\cos\mu - Y\sin\mu + T(\cos\alpha\sin\beta\sin\mu + \sin\alpha\cos\mu)\} - \frac{g}{V}\cos\gamma \tag{15a}$$

$$f_V = \frac{1}{mV}(-D + T\cos\alpha\cos\beta) \tag{15b}$$

where $g_\mu = -g\tan\beta\cos\mu\cos\gamma$, $g_\beta = g\sin\mu\cos\gamma$, and $g_\alpha = g\cos\mu\cos\gamma/\cos\beta$.

2.3 Aerodynamic Uncertainty Model

Generally, aerodynamics has the most influential uncertainties compared to the other components of the aircraft. Therefore, its effect should not be ignored. In this section the model of aerodynamic uncertainties are constructed.

Let us define the moment coefficient errors as $\Delta\mathbf{E}_0 = \mathbf{E}_0 - \hat{\mathbf{E}}_0$, $\Delta\mathbf{E} = \mathbf{E} - \hat{\mathbf{E}}$ where the upper hat on a parameter stands for its nominal value. Assume that the errors are bounded as

$$\begin{aligned} \|\Delta\mathbf{E}_0\|_2 &\le b_{E_0} \\ \|\Delta\mathbf{E}\|_2 &\le b_E \end{aligned} \tag{16}$$

The moment uncertainty mainly affects the angular velocity $\boldsymbol{\omega}$-dynamics, which will be discussed in Sec. 3. Likewise, the sideforce and lift error $\Delta_Y = Y - \hat{Y}$ and $\Delta_L = L - \hat{L}$ are modeled as

$$|\Delta_Y| \le b_Y \tag{17a}$$

$$|\Delta_L| \le b_L \tag{17b}$$

The force uncertainty mainly affects the aerodynamic angle $\mathbf{x}_2$ dynamics, which is modeled as

$$\mathbf{f}_2(\mathbf{x}, \boldsymbol{\delta}) = \hat{\mathbf{f}}_2 + \boldsymbol{\Delta}_2 \tag{18}$$

where $\boldsymbol{\Delta}_2 = \left[\Delta_\mu \; \Delta_\beta \; \Delta_\alpha\right]^\top$ with

$$\Delta_\mu = \frac{1}{mV}\{\Delta_Y\cos\mu\tan\gamma + \Delta_L(\tan\beta + \sin\mu\tan\gamma)\} \tag{19a}$$

$$\Delta_\beta = \frac{1}{mV}\Delta_Y \tag{19b}$$

$$\Delta_\alpha = \frac{1}{mV\cos\beta}\Delta_L \tag{19c}$$

By Eq. (18), $\mathbf{x}_2$-dynamics can be rewritten as follows.

$$\dot{\mathbf{x}}_2 = \hat{\mathbf{f}}_2(\mathbf{x}, \boldsymbol{\delta}) + \mathbf{G}_2(\mathbf{x})\,\boldsymbol{\omega} + \boldsymbol{\Delta}_2 \tag{20}$$

The overall equations of motion are summarized as a single state equation as

$$\dot{\mathbf{x}} = \mathbf{f}(\mathbf{x}, \delta_t, \boldsymbol{\delta}) \tag{21}$$

DOI: 10.13009/EUCASS2017-192

3. Control Allocation

Usually, aircraft control surfaces have highly nonlinear and coupled influence on aerodynamic moments L, M, and N. Moreover, they have constraints such as angle saturation and rate limit. These properties of actual inputs of the system (21) makes the design of a controller quite difficult. The linearization about the trim condition is a good alternative but it may result in too small region of attraction due to complex nonlinearity near ill flight condition. To resolve such problems, Control Allocation (CA) is adopted in this study. Although CA is often used to handle redundancy of a system when the number of actual inputs is larger than that of moment components, it is also an effective tool that covers the complex relation between actual inputs and controlled inputs, and constraints on the effectors. CA computes the efficient control inputs corresponding to the desired moment in optimization sense.

Among several types of CA being commonly applied to aircraft control, one of the most efficient formulation for the case is the mixed optimization. The mixed optimization problem can be formulated as

$$\boldsymbol{\delta}^* = \underset{(\boldsymbol{\delta},\dot{\boldsymbol{\delta}})\in H}{\operatorname{argmin}} \left\{ (\mathbf{E}_{des} - \mathbf{E}_A)^\top \mathbf{W}_d (\mathbf{E}_{des} - \mathbf{E}_A) + \boldsymbol{\delta}^\top \mathbf{W}_p \boldsymbol{\delta} \right\} \tag{22}$$

where $\mathbf{W}_d$, $\mathbf{W}_p$ are diagonal and positive definite matrices, and $H = \{(\boldsymbol{\delta}, \dot{\boldsymbol{\delta}}) | \boldsymbol{\delta}_m \le \boldsymbol{\delta} \le \boldsymbol{\delta}_M,\ \hat{\boldsymbol{\delta}}_m \le \dot{\boldsymbol{\delta}} \le \hat{\boldsymbol{\delta}}_M\}$. The objective function in Eq. (22) is a sum of weighted moment error and weighted control effort. At the extremum, the error between the desired moment $\mathbf{E}_{des}$ and the feasible aerodynamic moment $\mathbf{E}_A$ is moderated to be small enough and so is the control surface deflection $\boldsymbol{\delta}$ according to the weighting matrices $\mathbf{W}_d$ and $\mathbf{W}_p$. If $\left\|\mathbf{W}_p\right\| \ll \|\mathbf{W}_d\|$, i.e. the relative weight of moment error is larger than the control effort, the solution will yield a resultant moment closer to the desired value. The set H is the feasible set which accounts for the angle saturation and rate limit of the control surfaces. Thus, all the solutions must reside inside or boundary of the set. Once one or more control surfaces saturate, optimization finds the closest deflections tracking the desired moment.

Note from Eq. (8) that the term $\mathbf{C}_0$ and the coefficient $\mathbf{C}_\delta$ in Eq. (7) can be identified as

$$\mathbf{C}_0 = \mathbf{C}_0 (V, \alpha, \beta, P, Q, R) \tag{23a}$$

$$\mathbf{C}_\delta = \mathbf{C}_\delta (\alpha) \tag{23b}$$

according to Eq. (8). The coefficients use the value of states of each moment.

Aileron Lock

The aggressive use of aileron during the high angle of attack maneuver often leads to undesirable asymmetric stall due to excessive effective angle of attack. In this case, the use of aileron should be restricted until the angle of attack is sufficiently decreased. The problem can be easily handled by adjusting control surface weighting matrix $\mathbf{W}_p = \operatorname{diag}(w_e, w_a, w_r)$. If the weight corresponding to aileron, w_a, is increased far above the other weights, the size of the aileron deflection of the optimal solution will be sharply reduced. For this purpose, the sigmoid function is introduced as follows.

$$\sigma(x) := \frac{a}{1 + e^{-k(x-c)}} \tag{24}$$

In this study, the weight is designed as a function of angle of attack using the following sigmoid function.

$$w_a = 10^{\sigma(\alpha)} \tag{25}$$

where k_a is an appropriately chosen slope, α_c is a cutoff angle of attack which is chosen below the stall angle for safety. The shape of the function is shown in Fig. 1

3.1 Analytic Solution

If the solution is found in the interior of the feasible set, the solution can be written as a closed form. Let J be the objective function of Eq. (22) for some fixed states. Then, by Eq. (9)

$$f(\boldsymbol{\delta}) = \boldsymbol{\sigma}^\top \mathbf{W}_d \boldsymbol{\sigma} + \boldsymbol{\delta}^\top \mathbf{W}_p \boldsymbol{\delta} \tag{26}$$

where $\boldsymbol{\sigma} = \boldsymbol{\tau} - \mathbf{E}\boldsymbol{\delta}$, and $\boldsymbol{\tau} = \mathbf{E}_{des} - \mathbf{E}_0$. It is strictly convex with respect to $\boldsymbol{\delta}$ regardless of the rank of the coefficient matrix $\mathbf{E}$. Therefore, the extremum is unique, and the partial derivative of the objective function is zero at the point[7] as

$$\begin{aligned} \left.\frac{\partial f}{\partial \boldsymbol{\delta}}\right|_{\boldsymbol{\delta}=\boldsymbol{\delta}^*} &= 2\boldsymbol{\sigma}^\top \mathbf{W}_d \left.\frac{\partial \boldsymbol{\sigma}}{\partial \boldsymbol{\delta}}\right|_{\boldsymbol{\delta}=\boldsymbol{\delta}^*} + 2\boldsymbol{\delta}^{*\top} \mathbf{W}_p \\ &= -2(\boldsymbol{\tau} - \mathbf{E}\boldsymbol{\delta}^*)^\top \mathbf{W}_d \mathbf{E} + 2\boldsymbol{\delta}^{*\top} \mathbf{W}_p \\ &= 2\boldsymbol{\delta}^{*\top} \left(\mathbf{E}^\top \mathbf{W}_d \mathbf{E} + \mathbf{W}_p\right) - 2\boldsymbol{\tau}^\top \mathbf{W}_d \mathbf{E} \\ &= \mathbf{0} \end{aligned} \tag{27}$$

DOI: 10.13009/EUCASS2017-192

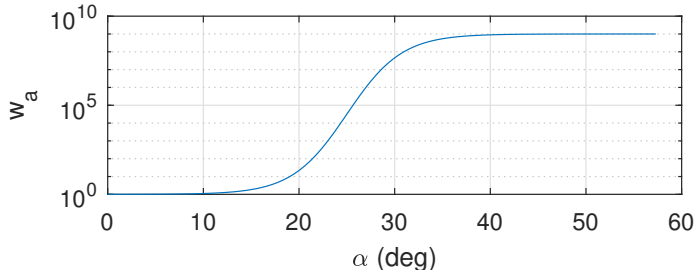

Figure 1: Sigmoid function shaping, w_a

Finally, $\boldsymbol{\delta}^*$ is obtained from Eq. (27) and written as

$$\boldsymbol{\delta}^*(\boldsymbol{\tau}) = \left(\mathbf{E}^\top \mathbf{W}_d \mathbf{E} + \mathbf{W}_p\right)^{-1} \mathbf{E}^\top \mathbf{W}_d \boldsymbol{\tau} \tag{28}$$

The aerodynamic moment coefficient corresponding to $\boldsymbol{\delta}^*$ is denoted as $\mathbf{E}_A{}^*$.

Although the analytic solution is valid only on the interior of H, the result is useful in application. In fact, the rate limit of control surfaces does not harmfully influence the response of the aircraft in the ordinary flight condition where abrupt control is not frequent because the actuator dynamics are generally much faster than the inherent dynamics driven by the aerodynamics of the aircraft. Therefore, the analytic solution, which has an extreme computational advantage and better accuracy, can be substituted for numerical solution.

3.2 Numerical Solution

In contrast to the rate limit, angle saturation should be considered in any flight condition. In other words, the control input obtained by clipping the signal (28) may degrade the stability of the aircraft. Likewise, in the upset condition, the rate limit may be an major obstruction to safe flight control. In such conditions, the solution satisfying all the constraints is strongly recommended, which can be obtained by numerical approach. As the function of Eq. (22) is in a quadratic form, the constrained optimization problem can be efficiently solved by numerical algorithms such as Sequential Quadratic Programming (SQP). The time derivative of deflections included in the set H is translated into a discrete form as follows.[8]

$$H = \{\boldsymbol{\delta} \,|\boldsymbol{\delta}_l \le \boldsymbol{\delta} \le \boldsymbol{\delta}_u\} \tag{29}$$

where

$$\begin{aligned} \boldsymbol{\delta}_u &= \min(\boldsymbol{\delta}_M, \boldsymbol{\delta}_p + \Delta t \hat{\boldsymbol{\delta}}_M) \\ \boldsymbol{\delta}_l &= \max(\boldsymbol{\delta}_m, \boldsymbol{\delta}_p + \Delta t \hat{\boldsymbol{\delta}}_m) \end{aligned} \tag{30}$$

for the sampling time Δt and the solution in the previous step $\boldsymbol{\delta}_p$.

3.3 Aerodynamic Uncertainty

If the CA error for the nominal model $\boldsymbol{\sigma} = \mathbf{E}_{des} - \hat{\mathbf{E}}_A$ is negligible, the resultant moment coefficient error is dominated by pure aerodynamic uncertainty as

$$\begin{aligned} \mathbf{E}_A - \mathbf{E}_{des} &= \hat{\mathbf{E}}_A - \mathbf{E}_{des} + \Delta\mathbf{E}_A \\ &\approx \Delta\mathbf{E}_A = \Delta\mathbf{E}_0 + \Delta\mathbf{E}\boldsymbol{\delta}^*(\boldsymbol{\tau}) \end{aligned} \tag{31}$$

If it is assumed further that the uncertainty of moment of inertia is ignored, Eq. (10) becomes

$$\dot{\boldsymbol{\omega}} = \mathbf{J}^{-1}\left(qS\left(\mathbf{E}_{des} + \Delta\mathbf{E}_A\right) - \boldsymbol{\Omega}\mathbf{J}\boldsymbol{\omega}\right) \tag{32}$$

Now, a new term $\mathbf{u}$ is introduced as an input to compensate the effect of the gyroscopic-coupling term $\boldsymbol{\Omega}\mathbf{J}\boldsymbol{\omega}$ and the moment of inertia $\mathbf{J}$ in Eq. (32) as

$$qS\,\mathbf{E}_{des} = \mathbf{J}\mathbf{u} + \boldsymbol{\Omega}\mathbf{J}\boldsymbol{\omega} \tag{33}$$

Then, the moment equation is simplified as follows.

$$\dot{\boldsymbol{\omega}} = \mathbf{u} + \boldsymbol{\Delta}_\omega \tag{34}$$

DOI: 10.13009/EUCASS2017-192

where $\mathbf{\Delta}_\omega = qS\mathbf{J}^{-1}\Delta\mathbf{E}_A$. Note that the uncertainty term has the following property.

$$\|\mathbf{\Delta}_\omega\| \leq b_\omega \tag{35}$$

where $b_\omega = b_q S\|\mathbf{J}^{-1}\|\left(b_{E_0} + b_E b_\delta\right)$, $b_q = \sup_{\mathbf{x}\in D} \rho V^2 \big/ 2$, $b_\delta = \sup_{\boldsymbol{\delta}\in H} \|\boldsymbol{\delta}^*\|$, and D is the flight domain.

4. Flight Controller

The objective of the flight control is to make the aircraft track the commanded inputs robustly in the presence of aerodynamic uncertainty. The command inputs are the roll rate P, the sideslip angle β, and the angle of attack α, i.e. $\mathbf{r} = [P_c\ \beta_c\ \alpha_c]^\top$ and the tracking error is defined as $\mathbf{e} = [e_P\ e_\beta\ e_\alpha]^\top = [P\ \beta\ \alpha]^\top - \mathbf{r}$. To design an adequate controller $\mathbf{u} = \mathbf{p}(\mathbf{x})$, the corresponding system with uncertainty is summarized as follows.

$$\dot{P} = \mathbf{i}^\top\mathbf{u} + \Delta_P \tag{36a}$$

$$\dot{\beta} = \hat{f}_\beta(\mathbf{x}, \boldsymbol{\delta}) + \mathbf{g}_\beta{}^\top\boldsymbol{\omega} + \Delta_\beta \tag{36b}$$

$$\dot{\alpha} = \hat{f}_\alpha(\mathbf{x}, \boldsymbol{\delta}) + \mathbf{g}_\alpha{}^\top\boldsymbol{\omega} + \Delta_\alpha \tag{36c}$$

where $\Delta_P = \mathbf{i}^\top\mathbf{\Delta}_\omega$.

First, the roll rate controller is designed as follows.

$$\mathbf{i}^\top\mathbf{p}(\mathbf{x}) = -k_P e_P + \dot{P}_c \tag{37}$$

With the control design, the roll rate error dynamics is exponentially stable without uncertainty.

$$\dot{e}_P = k_P e_P + \Delta_P \tag{38}$$

On the other hand, the backstepping control scheme is applied to β and α dynamics. By taking $\boldsymbol{\omega}$ as input, the virtual control $\boldsymbol{\omega} = \boldsymbol{\phi}(\mathbf{x})$ are designed for β and α, which stabilizes the system (36b) and (36c), as

$$\mathbf{g}_\beta{}^\top\boldsymbol{\phi}(\mathbf{x}) = -\hat{f}_\beta(\mathbf{x}, \boldsymbol{\delta}) - k_\beta e_\beta + \dot{\beta}_c \tag{39a}$$

$$\mathbf{g}_\alpha{}^\top\boldsymbol{\phi}(\mathbf{x}) = -\hat{f}_\alpha(\mathbf{x}, \boldsymbol{\delta}) - k_\alpha e_\beta + \dot{\alpha}_c \tag{39b}$$

The change of variables

$$z_\beta = \mathbf{g}_\beta{}^\top\boldsymbol{\omega} - \kappa_\beta(\mathbf{x}) \tag{40a}$$

$$z_\alpha = \mathbf{g}_\alpha{}^\top\boldsymbol{\omega} - \kappa_\alpha(\mathbf{x}) \tag{40b}$$

applies to Eq. (36) where $\kappa_\beta(\mathbf{x}) = \mathbf{g}_\beta^\top\boldsymbol{\phi}(\mathbf{x})$ and $\kappa_\alpha(\mathbf{x}) = \mathbf{g}_\alpha^\top\boldsymbol{\phi}(\mathbf{x})$. Notice that combining Eq. (36b), (36c), and (40) yields β and α error dynamics

$$\dot{e}_\beta = -k_\beta e_\beta + z_\beta + \Delta_\beta \tag{41a}$$

$$\dot{e}_\alpha = -k_\alpha e_\alpha + z_\alpha + \Delta_\alpha \tag{41b}$$

Using

$$\mathrm{V} = \left\{e_P{}^2 + e_\beta{}^2 + e_\alpha{}^2 + k_z\left(z_\beta{}^2 + z_\alpha{}^2\right)\right\}\Big/2 \tag{42}$$

as a Lyapunov function candidate, its derivative can be obtained as follows.

$$\begin{aligned}\dot{\mathrm{V}} = &-k_P e_P{}^2 - k_\beta e_\beta{}^2 - k_\alpha e_\alpha{}^2 \\ &+z_\beta\left\{e_\beta + k_z\left(\dot{\mathbf{g}}_\beta^\top\boldsymbol{\omega} - \dot{\kappa}_\beta(\mathbf{x}) + \mathbf{g}_\beta{}^\top\mathbf{u}\right)\right\} + z_\alpha\left\{e_\alpha + k_z\left(\dot{\mathbf{g}}_\alpha^\top\boldsymbol{\omega} - \dot{\kappa}_\alpha(\mathbf{x}) + \mathbf{g}_\alpha{}^\top\mathbf{u}\right)\right\} \\ &+e_P\Delta_P + e_\beta\Delta_\beta + e_\alpha\Delta_\alpha + k_\beta z_\beta\mathbf{g}_\beta{}^\top\mathbf{\Delta}_\omega + k_\alpha z_\alpha\mathbf{g}_\alpha{}^\top\mathbf{\Delta}_\omega\end{aligned} \tag{43}$$

where k's are positive constant parameters. The derivatives $\dot{\mathbf{g}}$ and $\dot{\kappa}$ remain intact where their subscripts are omitted for simplicity. The former can be directly obtained by the relation $\dot{\mathbf{g}} = \frac{\partial\mathbf{g}}{\partial\mathbf{x}}\mathbf{f}(\mathbf{x})$ and the function is denoted as $\bar{\mathbf{g}}(\mathbf{x})$. However, deriving the analytical derivative of latter one is extremely complicated and it is rarely worth a labor. Thus, in this study, it is handled by introducing two low-pass filters and the filter states are used as an approximated derivative, which are denoted as $\bar{\kappa}$.

DOI: 10.13009/EUCASS2017-192

Reminding $\mathbf{u} = \mathbf{p}(\mathbf{x})$, by choosing

$$k_z \mathbf{g}_\beta^\top \mathbf{p}(\mathbf{x}) = e_\beta k_z \left(\bar{\kappa}_\beta - \bar{\mathbf{g}}_\beta^\top \boldsymbol{\omega}\right) - n_\beta z_\beta \tag{44a}$$

$$k_z \mathbf{g}_\alpha^\top \mathbf{p}(\mathbf{x}) = e_\alpha k_z \left(\bar{\kappa}_\alpha - \bar{\mathbf{g}}_\alpha^\top \boldsymbol{\omega}\right) - n_\alpha z_\alpha \tag{44b}$$

Eq. (43) can be rewritten as

$$\begin{aligned} \dot{\mathrm{V}} &= -k_P {e_P}^2 - k_\beta {e_\beta}^2 - k_\alpha {e_\alpha}^2 - n_\beta {z_\beta}^2 - n_\alpha {z_\alpha}^2 \\ &\quad + e_P \Delta_P + e_\beta \Delta_\beta + e_\alpha \Delta_\alpha + k_\beta z_\beta \mathbf{g}_\beta^\top \boldsymbol{\Delta}_\omega + k_\alpha z_\alpha \mathbf{g}_\alpha^\top \boldsymbol{\Delta}_\omega \\ &\leq -k_P {e_P}^2 - k_\beta {e_\beta}^2 - k_\alpha {e_\alpha}^2 - n_\beta {z_\beta}^2 - n_\alpha {z_\alpha}^2 \\ &\quad + |e_P||\Delta_P| + \left|e_\beta\right|\left|\Delta_\beta\right| + |e_\alpha||\Delta_\alpha| + k_\beta \left|z_\beta\right| \left\|\mathbf{g}_\beta\right\| \|\boldsymbol{\Delta}_\omega\| + k_\alpha |z_\alpha| \|\mathbf{g}_\alpha\| \|\boldsymbol{\Delta}_\omega\| \end{aligned} \tag{45}$$

which shows that the origin $\left(e_P = 0,\ e_\beta = 0,\ e_\alpha = 0,\ z_\beta = 0,\ z_\alpha = 0\right)$ is ultimately bounded.[9]

Finally, by combining Eq. (37) and Eq. (44)

$$\begin{bmatrix} \mathbf{i}^\top \\ k_z \mathbf{g}_\beta{}^\top \\ k_z \mathbf{g}_\alpha{}^\top \end{bmatrix} \mathbf{p}(\mathbf{x}) = \begin{bmatrix} -k_P e_P + \dot{P}_c \\ e_\beta k_z \left(\bar{\kappa}_\beta - \bar{\mathbf{g}}_\beta^\top \boldsymbol{\omega}\right) - n_\beta z_\beta \\ e_\alpha k_z \left(\bar{\kappa}_\alpha - \bar{\mathbf{g}}_\alpha^\top \boldsymbol{\omega}\right) - n_\alpha z_\alpha \end{bmatrix} \tag{46}$$

the controller $\mathbf{p}(\mathbf{x})$ can be explicitly obtained where the matrix in the left-hand side is always invertible in the flight domain.

4.1 Pilot Command Mapping

For manned aerial vehicles, the flight control commands are generated from pilot's stick and pedal inputs. Once the signal is received by flight control computer, the commands are typically mapped to roll rate and aerodynamic angles. The mapping is summarized in Table 1 where ν_{lat}, ν_{lon}, and ν_{yaw} represent the pilot command signals and h_P, h_α, and h_β are increasing functions being saturated at the each boundary of corresponding ranges.

Table 1: Pilot command mapping

Command	Stick left/right	Stick forward/backward	Rudder pedal
Mapping	$P_c = h_P(\nu_{\text{lat}})$	$\alpha_c = h_\alpha(\nu_{\text{lon}})$	$\beta_c = h_\beta\left(\nu_{\text{yaw}}\right)$
Range	$\left[\hat{P}_m,\ \hat{P}_M\right]$	$[\hat{\alpha}_m,\ \hat{\alpha}_M]$	$\left[\hat{\beta}_m,\ \hat{\beta}_M\right]$

4.2 Flight Envelope Protection

The flight envelope considered in this study consists of β, α, and the normal load factor n_z and its specification is summarized in Table 2.

Table 2: Safe flight envelope

Parameter	β (deg)	α (deg)	n_z
Range	$[\beta_m,\ \beta_M]$	$[\alpha_m,\ \alpha_M]$	$[n_m,\ n_M]$

Because the controller ensures that the state variables robustly track commanded inputs, for β and α, their envelope exceedance is prevented due to pilot command mapping developed in Sec. 4.1 by letting the command range included in the envelope range with a safe margin. However, the normal load factor envelope is not yet guaranteed to remain inside the safe envelope during the flight. In fact, the normal load factor can be easily protected by adjusting angle of attack envelope. The normal load factor is defined as follows.

$$n_z = \frac{L}{W} \approx \frac{\rho S V^2}{2mg} C_{L_0}(\alpha) \tag{47}$$

Consider a truncation of the lift coefficient $f_{C_L} : [\alpha_m,\ \alpha_M] \to [C_{L_0}(\alpha_m),\ C_{L_0}(\alpha_M)]$ given by $f_{C_L}(\alpha) = C_{L_0}(\alpha)$. As C_{L_0}

DOI: 10.13009/EUCASS2017-192

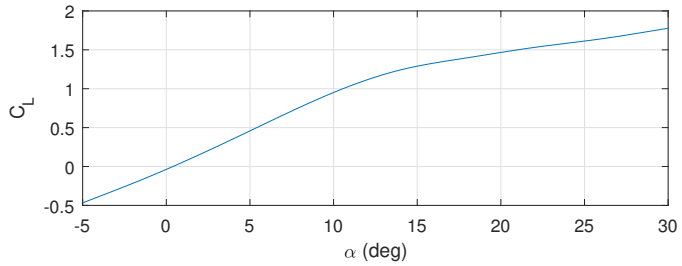

Figure 2: Truncation of lift coefficient, f_{C_L}

is strictly increasing, the inverse of f_{C_L} exists and α can be written with respect to n_z for the sufficiently large dynamic pressure $q = \rho V^2/2$ such that $mgn_z/q \in [C_{L_0}(\alpha_m),\ C_{L_0}(\alpha_M)]$.

$$\alpha = f_{C_L}^{-1}\left(\frac{2mg}{\rho S V^2} n_z\right) \tag{48}$$

Then, the safe angle of attack envelope regarding the normal load factor protection can be written as follows.

$$\alpha_{c,\text{sat}} \in \left[\max\left(\alpha_m,\ f_{C_L}^{-1}\left(\frac{2mg}{\rho S V^2} n_m\right)\right), \min\left(\alpha_M,\ f_{C_L}^{-1}\left(\frac{2mg}{\rho S V^2} n_M\right)\right)\right] \tag{49}$$

Then any angle of attack command exceeding the interval is made saturated at the boundary.

5. Simulation Results

The controller proposed in Sec. 4 is applied to the F/A-18 HARV model and the simulation results are represented in this section. A total of four simulations are performed to show the robustness of the controller and performance of flight envelope protection. The flight envelope to be protected is summarized in Table 3. The uncertainty is applied to the moment coefficients and their bounds are $b_{E_0} = 0.02$ and $b_E = 0.05$.

Table 3: Safe flight envelope

Parameter	P	β	α	n_z
Range	$[-45,\ 45]$ (deg/s)	$[-5,\ 30]$ (deg)	$[-15,\ 15]$ (deg)	$[-1,\ 3]$

5.1 Robustness of Backstepping Controller

Two simulation results are represented to show the robustness of the controller. The load factor envelope protection is not applied in this section. The command inputs are summarized in Table 4.

Table 4: Conditions for Simulation 1 and 2

Command	P_c (deg/s)	β_c (deg)	α_c (deg)
Simulation 1	-30	0	25
Simulation 2	-30	0	$10\sin t + 5$

The results of Simulation 1 and 2 are shown in Figs. 3 and 4 where the subcript 'nom' and 'unc' denote the nominal aircraft model and the aircraft model with aerodynamic uncertainty, respectively. Note that the same controller is applied to both case. The overall control performance is acceptable even if the total velocity V_T suddenly varies with time owing to the nonlinear backstepping control scheme. The control allocation optimization error f^* remains at a low value during the maneuver, which means that the desired moment is achieved by the control allocation. P and β exhibit large excursion because the given uncertainty condition is set extremely harsh compared to the general flight condition. Furthermore, the command inputs of the simulations are also demanding; the commands are called barrel-roll. Nevertheless, the results are permissible in that angle of attack maintains relatively small deviation from the commanded value, which is due to the large control gain assigned to the angle of attack.

DOI: 10.13009/EUCASS2017-192

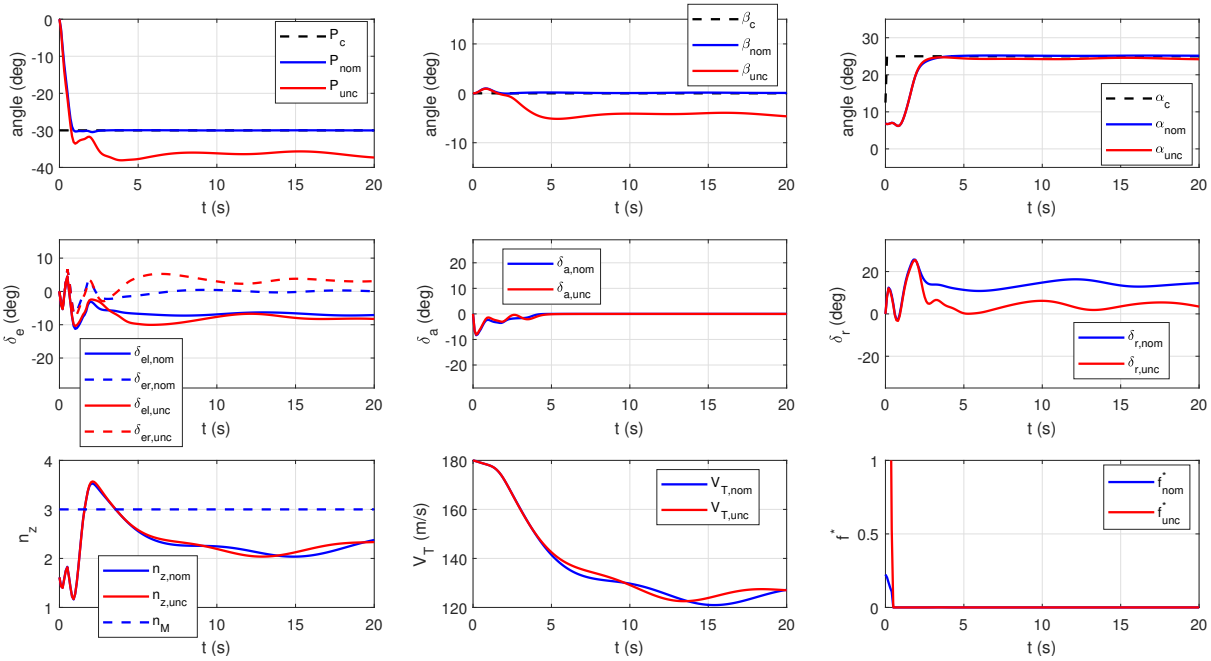

Figure 3: Result of Simulation 1

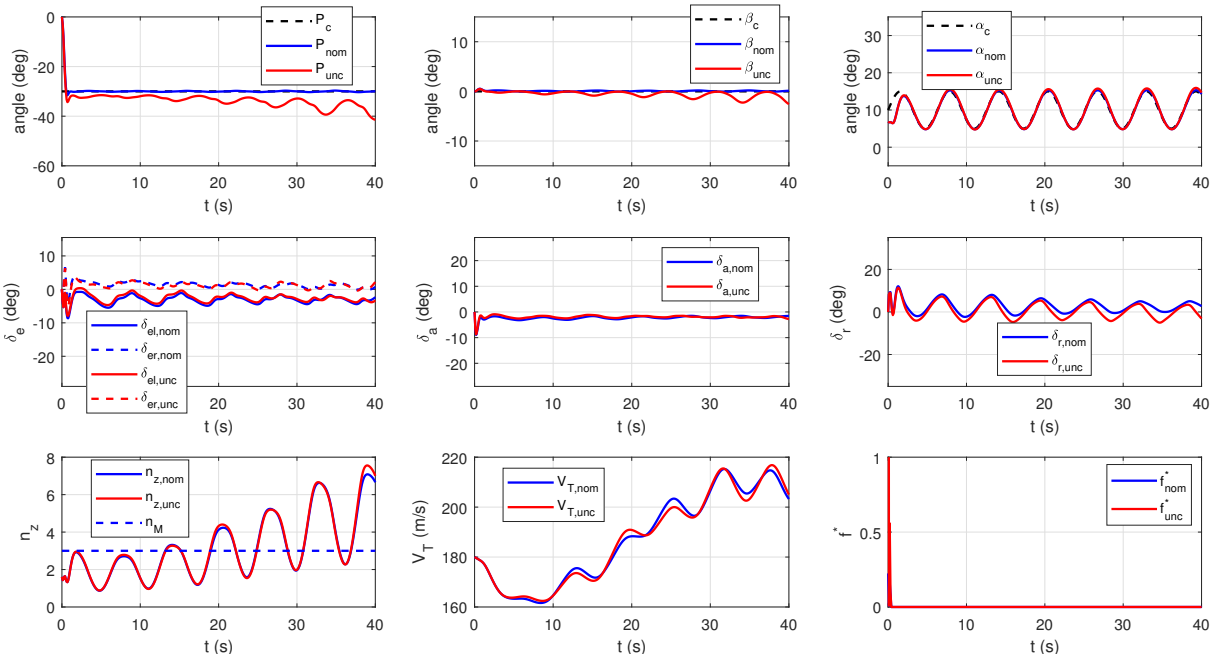

Figure 4: Result of Simulation 2

DOI: 10.13009/EUCASS2017-192

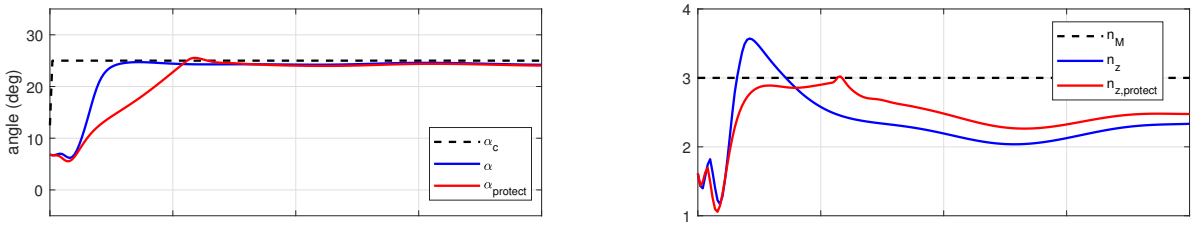

Figure 5: Result of Simulation 3

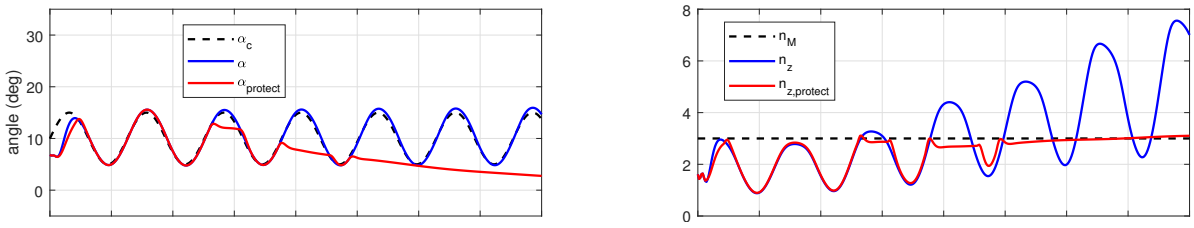

Figure 6: Result of Simulation 4

It is worth noting that, in both cases, the normal load factor exceeded by far the safe range noted in Table 3. The situation can be avoided by applying normal load factor envelope protection, whose result is presented in the following section.

5.2 Normal Load Factor Envelope Protection

As stated previously, the angle of attack and the sideslip angle envelope are consequently protected by the pilot command mapping. In this section, the performance of normal load factor envelope protection under aerodynamic uncertainty is studied.

The command inputs are given the same as Simulation 1 and 2. However, a significant difference occurs at the normal load factor curves. In Fig. 5, the normal load factor curve without protection shows the overshoot while the result with envelope protection shows that the curve is confined inside the safe envelope. A drastic result is shown in Fig. 6. While tracking sinusoidal wave command of the angle of attack, the curve without protection exceeds the envelope intermittently and its magnitude grows as time advances. However, the curve with envelope protection never exceeds the envelope throughout the simulation. Though the angle of attack temporarily deviates from its commanded value, it is more important to keep all the states inside the safe flight envelope.

6. Conclusions

In this study, a nonlinear flight controller with a flight envelope protection based on backstepping control scheme is designed. The aerodynamic uncertainty model was developed and its effect on the aircraft stability was considered. Furthermore, it was shown that the origin of the error dynamics is ultimately bounded with the type of uncertainty by using Lyapunov stability theorem, which shows the certain robustness of the controller. Numerical simulation shows the performance of the proposed control scheme. The robust tracking of angle of attack and sideslip angle ensures that the states are captured in the safe flight envelope. The normal load factor envelop protection law is also shown to be effective during the aggressive maneuver.

Acknowledgments

This work was supported by the project "Development of Aircraft Reconfiguration Control Law for Sensor-Actuator Faults" grant funded by the Korean Aerospace Industries, LTD.

DOI: 10.13009/EUCASS2017-192

References

[1] Wilborn, J. and Foster, J., "Defining Commercial Transport Loss-of-Control: A Quantitative Approach," *AIAA Atmospheric Flight Mechanics Conference and Exhibit*, Providence, RI, 2004, p. 4811.

[2] Chongvisal, J., Tekles, N., Xargay, E., Talleur, D., Kirlik, A., and Hovakimyan, N., "Loss-of-Control Prediction and Prevention for NASA's Transport Class Model," *AIAA Guidance, Navigation, and Control Conference*, National Harbor, MD, 2014.

[3] Farrell, J., Sharma, M., and Polycarpou, M., "Backstepping-based Flight Control with Adaptive Function Approximation," *Journal of Guidance, Control, and Dynamics*, Vol. 28, No. 6, 2005, pp. 1089–1102.

[4] Sonneveldt, L., Chu, Q., and Mulder, J., "Nonlinear Flight Control Design Using Constrained Adaptive Backstepping," *Journal of Guidance, Control, and Dynamics*, Vol. 30, No. 2, 2007, pp. 322–336.

[5] Tekles, N., Holzapfel, F., Xargay, E., Choe, R., Hovakimyan, N., and Gregory, I. M., "Flight Envelope Protection for NASA's Transport Class Model," *AIAA Guidance, Navigation, and Control Conference*, National Harbor, MD, 2014.

[6] Horn, J., Calise, A., and Prasad, J., "Flight Envelope Limiting Systems Using Neural Networks," *23rd Atmospheric Flight Mechanics Conference*, 1998, p. 4459.

[7] Boyd, S. and Vandenberghe, L., *Convex Optimization*, Cambridge University Press, Cambridge, 2004.

[8] Levine, W. S., *The Control Handbook: Control System Fundamentals*, CRC press, Boca Raton, FL, 2010.

[9] Hassan, K. K., *Nonlinear Systems*, Prentice Hall, Upper Saddle River, NJ, 2002.